scientific reports

OPEN

Super fine cerium hydroxide abrasives for SiO₂ film chemical mechanical planarization performing scratch free

Young-Hye Son[1], Gi-Ppeum Jeong[2], Pil-Su Kim[1], Man-Hyup Han[1], Seong-Wan Hong[1], Jae-Young Bae[3], Sung-In Kim[1], Jin-Hyung Park[4] & Jea-Gun Park[1,2✉]

Face-centered-cubic crystallized super-fine (~ 2 nm in size) wet-ceria-abrasives are synthesized using a novel wet precipitation process that comprises a Ce^{4+} precursor, $C_3H_4N_2$ catalyst, and NaOH titrant for a synthesized termination process at temperature of at temperature of 25 °C. This process overcomes the limitations of chemical–mechanical-planarization (CMP)-induced scratches from conventional dry ceria abrasives with irregular surfaces or wet ceria abrasives with crystalline facets in nanoscale semiconductor devices. The chemical composition of super-fine wet ceria abrasives depends on the synthesis termination pH, that is, $Ce(OH)_4$ abrasives at a pH of 4.0–5.0 and a mixture of CeO_2 and $Ce(OH)_4$ abrasives at a pH of 5.5–6.5. The $Ce(OH)_4$ abrasives demonstrate better abrasive stability in the SiO_2-film CMP slurry than the CeO_2 abrasives and produce a minimum abrasive zeta potential (~ 12 mV) and a minimum secondary abrasive size (~ 130 nm) at the synthesis termination pH of 5.0. Additionally, the abrasive stability of the SiO_2-film CMP slurry that includes super-fine wet ceria abrasives is notably sensitive to the CMP slurry pH; the best abrasive stability (i.e., a minimum secondary abrasive size of ~ 130 nm) is observed at a specific pH (6.0). As a result, a maximum SiO_2-film polishing rate (~ 524 nm/min) is achieved at pH 6.0, and the surface is free of stick-and-slip type scratches.

Recently, dynamic random-access memory (DRAM) has been scaled down to ~ 1 nm per year, and NAND-flash memory has been stacked with ~ floors per two years[1–8]. Additionally, logic devices for application processors (APs), central processing units (CPUs), and graphic processing units (GPUs) have been scaled down from 7 nm to 5, 3, and 2 nm, respectively[9–11]. The scaling-down speed of nanoscale semiconductor devices has slowed down, owing to the lithography limit as a result of large surface topography and device structure complexity[12–17]. In particular, the need for chemical mechanical planarization (CMP) for the removal of such surface topography has increased in nanoscale semiconductor device fabrication[18–21]. Among the CMP processes, shallow trench isolation (STI) CMP is an essential fabrication process for all nanoscale semiconductor devices, and poly-Si stop CMP is also an inevitable fabrication process for three-dimensional (3D) NAND-flash memory[22–26].

Historically, both STI and poly-Si stop CMP have been performed using a nanoscale (~ 100 nm in size) crystalline cerium oxide abrasive (CeO_2)-based CMP slurry. In particular, the surface morphology of crystalline cerium oxide abrasives has recently changed from a sharp surface (i.e., dry cerium oxide abrasives) to a crystalline-facet surface (i.e., wet cerium oxide abrasives) with {100}, {110}, and {111} to minimize the CMP-induced scratches produced by the stick-and-slip mechanism, as shown in Figs. 1a–b and S1. Additionally, the size of wet cerium oxide abrasives with crystalline-facet surfaces has been rapidly reduced because the allowable size of CMP-induced scratches has significantly decreased with the scaling down of nanoscale semiconductor devices[27–31]. However, CMP performance has faced the fundamental issue of a trade-off between the SiO_2, Si_3N_4, or poly-Si film polishing rate and the remaining CMP induced scratches; that is, a smaller wet cerium oxide abrasive size leads to fewer remaining CMP-induced scratches and a lower film polishing rate, as shown in Fig. 1. This trade-off meets the application limit of a wet cerium oxide abrasive-based CMP slurry for the further scaling-down of nanoscale DRAM, 3D NAND-flash, and logic devices.

[1]Department of Nanoscale Semiconductor Engineering, Hanyang University, Seoul 04763, Republic of Korea. [2]Department of Electronics and Communications Engineering, Hanyang University, Seoul 04763, Republic of Korea. [3]Department of Energy Engineering, Hanyang University, Seoul 04763, Republic of Korea. [4]UB Materials Inc., Yongin, Gyeonggi-do 17162, Republic of Korea. ✉email: parkjgL@hanyang.ac.kr
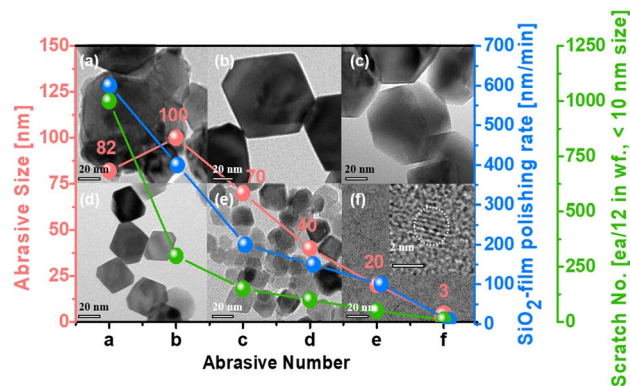
Figure 1. Dependencies of the SiO$_2$ film polishing rate and allowable scratch number on the size of dry or wet CeO$_2$ abrasives. (**a**) 82 nm dry CeO$_2$ abrasives, (**b**) 100 nm, (**c**) 70 nm, (**d**) 40 nm, (**e**) 20 nm, and (**f**) 3 nm wet CeO$_2$ abrasives. Dry CeO$_2$ abrasives with an irregular surface are produced via a milling process of cerium carbonate, whereas wet ceria abrasives containing f.c.c.-crystalline facets are synthesized by a conventional wet precipitation process at 60–80 °C.
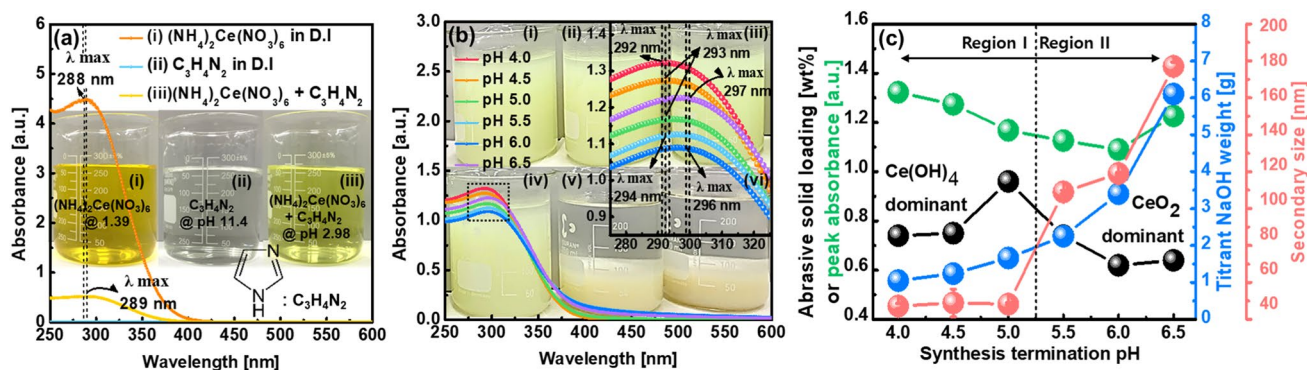
Figure 2. Dependencies of chemical and material properties of super-fine wet ceria abrasives on synthesis termination pH. (**a**) Chemical solution color of (i) precursor (NH$_4$)$_2$Ce(NO$_3$)$_6$ dissolved in DI water, (ii) C$_3$H$_4$N$_2$ dissolved in DI water, and (iii) (NH$_4$)$_2$Ce(NO$_3$)$_6$ and C$_3$H$_4$N$_2$ dissolved in DI water. (**b**) Peak absorption wavelength and absorbance dependent on synthesis termination pH. Beaker (i), (ii), (iii), (iv), (v), and (vi) of the D.I. solutions with dispersed super-fine wet ceria abrasives were terminated at a pH of 4.0, 4.5, 5.0, 5.5, 6.0, and 6.5, respectively, following a synthesis. (**c**) Titrant NaOH weight, abrasive solid loading, peak absorbance, and secondary abrasives size, dependent on synthesis termination pH.

In this study, we developed crystalline cerium hydroxide (CeOH$_4$) abrasives with a size of ~2 nm (called super-fine CeOH$_4$ abrasives) at temperature of 25 °C. This is an alternative to crystalline cerium oxide (CeO$_2$) abrasives, which are produced via wet precipitation synthesis using a Ce^{4+} precursor, catalyst for enhancing Ce^{4+} solubility, and pH titrant. Note that crystalline CeO$_2$ abrasives are synthesized using a Ce^{4+} seed precursor and Ce^{3+} growth precursor at 60–80 °C, as shown in Fig. S2. First, we demonstrated in detail the mechanism by which super-fine wet Ce(OH)$_4$ abrasives are synthesized via wet precipitation using a Ce^{4+} precursor, catalyst and pH titrant. In addition, we use a CMP slurry with super-fine wet Ce(OH)$_4$ abrasives to investigate the dependence of the absorbance of wet cerium hydroxide abrasives, secondary abrasive size, the zeta potential of wet cerium hydroxide abrasives, and CMP performance on the synthesis termination pH and CMP slurry pH.

Results

Super-fine wet cerium hydroxide (Ce(OH)$_4$)) abrasive synthesis mechanism. Nanoscale (5–100 nm in size) wet ceria abrasives were typically synthesized using Ce^{3+} and Ce^{4+} precursors at >60 °C, as shown in Fig. S2. However, super-fine (~2 nm in size) wet ceria abrasives were synthesized using only the Ce^{4+} precursor at temperature of 25 °C. The synthesis mechanism of super-fine wet ceria abrasives can be analyzed by observing the color of the abrasives in a solution after synthesis. Ammonium cerium nitrate ((NH$_4$)$_2$Ce(NO$_3$)$_6$)) was utilized as a Ce^{4+} precursor and imidazole (C$_3$H$_4$N$_2$) as a catalyst to enhance the Ce^{4+} solubility. Both were dissolved in deionized (DI) water; the dissolved (NH$_4$)$_2$Ce(NO$_3$)$_6$ exhibited a transparent orange color, and C$_3$H$_4$N$_2$ was colorless, as shown in beakers (i) and (ii) of Fig. 2a. After mixing (NH$_4$)$_2$Ce(NO$_3$)$_6$ with C$_3$H$_4$N$_2$, the mixed chemical presented a transparent and bright yellow color, as shown in beaker (iii) of Fig. 2a. The absorbance of the (NH$_4$)$_2$Ce(NO$_3$)$_6$ solution (at pH 1.39) and the mixed (NH$_4$)$_2$Ce(NO$_3$)$_6$ solution (at pH 2.98) and

$C_3H_4N_2$ solution (at pH 11.40) peaked at wavelengths of 288 nm and 289 nm, respectively. Note that the $C_3H_4N_2$ chemical was added to the $(NH_4)_2Ce(NO_3)_6$ solution at a flow rate of 10 ml/min, and the two chemicals were mixed via stirring. Then, sodium hydroxide (NaOH) was added to titrate the pH of the mixed chemical (i.e., 4.0, 4.5, 5.0, 5.5, 6.0, and 6.5), which is called a synthesis termination process. The color of the solution containing abrasives after the synthesis termination process was dependent on the termination pH, as shown in the beakers in Fig. 2b. It changed from opaque and bright yellow (beaker (i) of Fig. 2b) to pale yellow (beaker (vi) of Fig. 2b) when the synthesis termination pH was adjusted from 4.0 to 6.5. In particular, at a pH above 6.0, the abrasives in the solution were completely sediment. To investigate the detailed color of the synthesized abrasives, the solutions including the abrasives were centrifuged three times and dispersed in DI water; the pH values were between 3.10–3.21. At a pH of 4.0, the synthesized abrasives were bright yellow, as shown in the centrifugal bottle of Fig. S3a. This is the typical color of $Ce(OH)_4$ powder, as shown in Fig. S4a, which indicates that the chemical composition of the synthesized abrasives at a pH of 4.0 is $Ce(OH)_4$. However, at a pH 6.5, the abrasives exhibited a pale yellow color, as shown in the centrifugal bottle in Fig. S3f, which is the typical color of CeO_2 powder, as shown in Fig. S4b. This indicates that the chemical composition of the synthesized abrasives (pH 6.5) was CeO_2. In addition, from a pH of 4.5 to 6.0, the color of the synthesized abrasives changed from bright yellow to pale yellow, which implies that their chemical composition is a mixture of $Ce(OH)_4$ and CeO_2, as shown in the centrifugal bottle in Fig. S3b–e. In particular, the chemical composition of the synthesized abrasives at a pH of 6.0 would be almost CeO_2. These results indicate that the color of the synthesized abrasives (i.e., the chemical composition of super-fine wet ceria abrasives) is dominantly dependent on the synthesis termination process pH. The difference between CeO_2 and $Ce(OH)_4$ can be recognized by analyzing the chemical composition between them using XPS, as shown in Fig. S5. The relative XPS peak signals of CeO_2, $Ce(OH)_4$ and Ce_2O_3 are found at 529.29, 530.79, and 532.29 eV, respectively. We prepare 3 samples such as commercial CeO_2 (UB materials Co.), commercial $Ce(OH)_4$ (Sigma Aldrich Co.), and $Ce(OH)_4$ (our synthesis) abrasives. The sequence of a higher relative XPS intensity of CeO_2 was followed by commercial CeO_2, commercial $Ce(OH)_4$, and $Ce(OH)_4$ abrasives. Otherwise, the order of a higher relative XPS intensity of $Ce(OH)_x$ was followed by $Ce(OH)_4$, commercial $Ce(OH)_4$, and commercial CeO_2 abrasives. Thus, these results indicate that the chemical composition of $Ce(OH)_4$ is different from that of CeO_2. From a pH of 4.0 to 5.0 (region I), the main synthesized abrasives are the $Ce(OH)_4$ abrasives; however, from a pH of 5.5 to 6.5 (region II), a mixture of the $Ce(OH)_4$ and CeO_2 abrasives are evident. In particular, the synthesized abrasives at a pH of 6.5 are principally CeO_2 abrasives.

The dependence of the titrant (NaOH) weight and abrasive solid loading after synthesis on the synthesis termination pH were investigated to estimate the dispersion ability of super-fine wet ceria abrasives in a DI solution. The NaOH weight exponentially increased with the synthesis termination pH, which is a typical titration method; it increased from 1.05 to 6.01 g when the pH increased from 4.0 to 6.5, as shown in Fig. 2c. Additionally, the abrasive solid loading weight after synthesis (~ 0.96 wt%) peaked at a pH of 5.0. Between a pH of 4.0 and 5.0 (region I), the abrasive solid loading weight considerably increased from 0.74 to 0.96 wt%; therefore, the $Ce(OH)_4$ growth rate increased with the synthesis termination pH because it was enhanced with the titrant NaOH weight. Hence, the $Ce(OH)_4$ abrasive color in all solutions was bright yellow, as shown in beakers (i)–(iii) of Fig. 2b, because the $Ce(OH)_4$ abrasives solid loading weight increased with the synthesis termination pH. However, between a pH of 5.5 and 6.5 (region II), the abrasive solid loading weight significantly decreased from 0.74 to 0.64 wt%. This implies that the CeO_2 abrasive growth rate in the solution is higher than that of $Ce(OH)_4$ because the CeO_2 abrasives and H_2O molecules are produced via the reaction of the $Ce(OH)_4$ abrasives with OH^- in the solution. It should be noted that the CeO_2 molecular weight (172 g/mol) is lighter than that of $Ce(OH)_4$ (208 g/mol). Thus, the abrasive solid loading weight decreased as the synthesis termination process pH increased. As a result, the abrasive color varied from dark bright yellow to pale yellow, as shown in beakers (iv)–(vi) of Figs. 3b, S3d–f. The dependency of the abrasive solid loading after synthesis on the synthesis termination pH indicates that the abrasive solid loading weight (~ 0.96 wt%) peaked at a specific synthesis termination pH (i.e., pH 5.0) because a maximum amount of $Ce(OH)_4$ abrasives was produced at a pH of 5.0.

The dependency of the abrasive solid loading weight after three centrifugation cycles on the synthesis termination pH was confirmed by observing the dependencies of the peak absorbance wavelength and the peak absorbance in the DI solution that included abrasives on the synthesis termination pH. The peak absorbance wavelength increased continuously from 292 to 297 nm when the synthesis termination pH increased from 4.0 to 6.5, as shown in the inset of Fig. 2b. This indicates that the chemical composition of the abrasives transformed from $Ce(OH)_4$ to CeO_2 and is well correlated with the dependency of the abrasive color on the synthesis termination pH in beakers (i)–(vi) of Fig. 2b. Note that the peak absorbance wavelengths of the $Ce(OH)_4$ and CeO_2 abrasives were at ~ 293 and ~ 297 nm, respectively[32–34]. Moreover, the peak absorbance decreased linearly from 1.325 to 1.090 a.u. when the synthesis termination pH increased from 4.0 to 6.0; it then abruptly increased to 1.226 a.u. at the synthesis termination pH of 6.5, which is likely related to the increase in the secondary abrasive size dispersed in a DI solution. Furthermore, the secondary abrasive size in a DI water solution was sustained at ~ 48 nm between the synthesis termination pH values of 4.0 and 5.0 (region I), which indicates that the super-fine abrasives were well dispersed, as shown Fig. 2c. For a further pH increase from 5.5 to 6.5, the secondary abrasive size exponentially increased with the synthesis termination pH; thus, the abrasive dispersion ability decreased at the synthesis termination pH of 5.5–6.5 (region II). The dependence of the abrasive secondary size on the synthesis termination pH implies that the $Ce(OH)_4$ abrasives in the DI water solution were well dispersed between the termination pH values of 4.0 and 5.0 (region I). However, the CeO_2 abrasives dispersed in the solution with a pH above 5.5 (region II) became further agglomerated as the pH increased. The absorbance of a solution that contains abrasives generally depends on the dispersant degree of the abrasives in the solution; that is, a higher abrasive dispersant degree in a solution results in a lower abrasive peak absorbance. Thus, the dependency of the peak absorbance in a solution that includes abrasives on the synthesis termination pH is
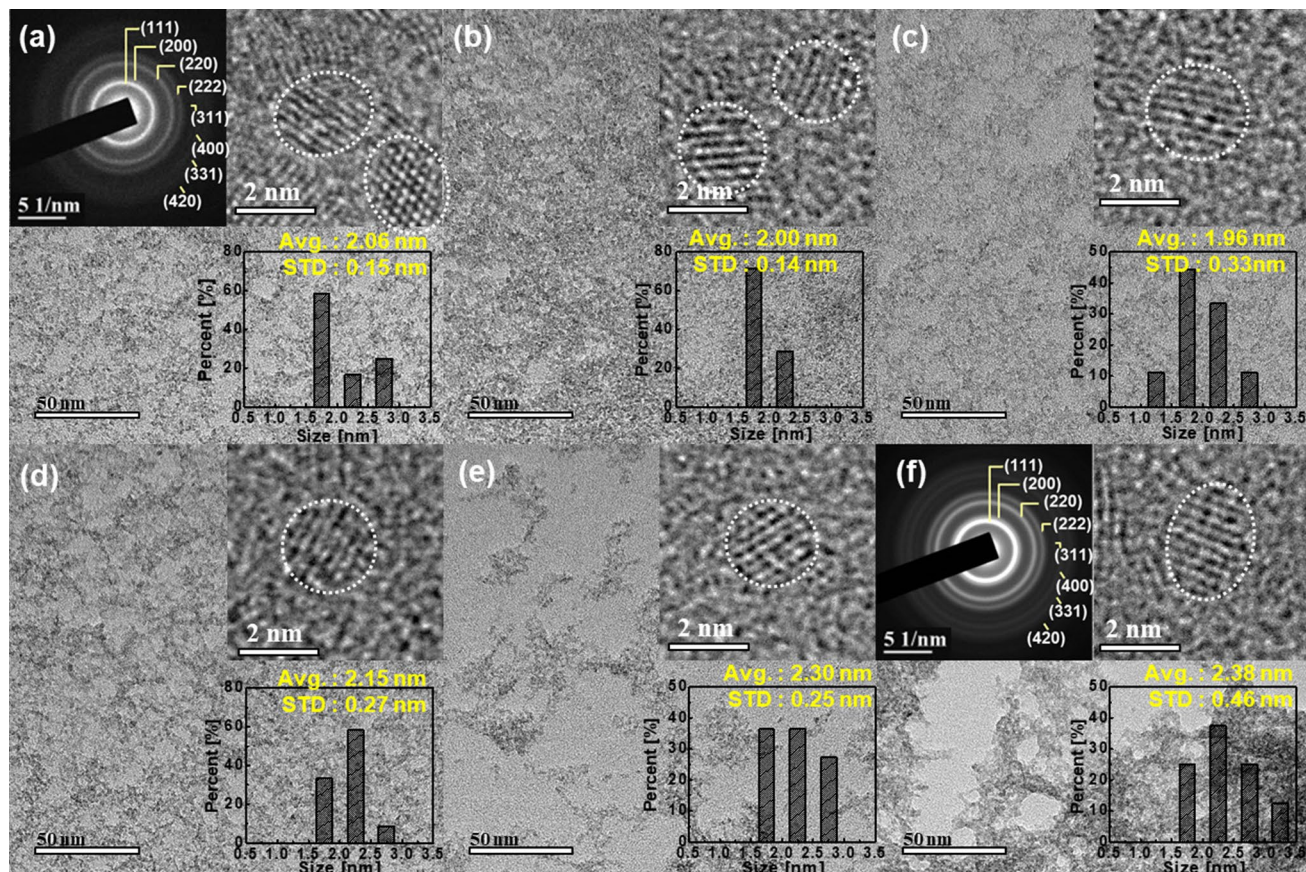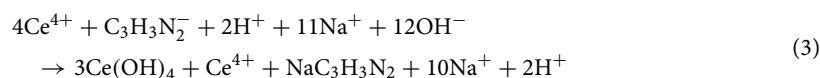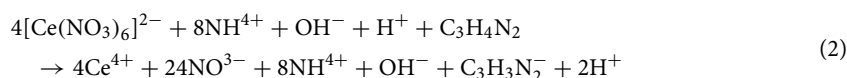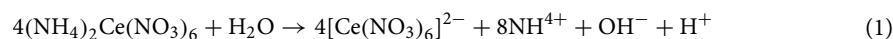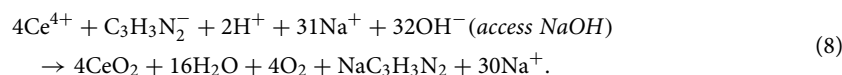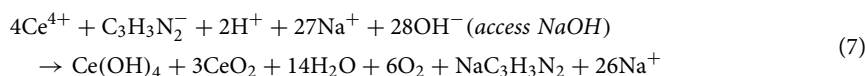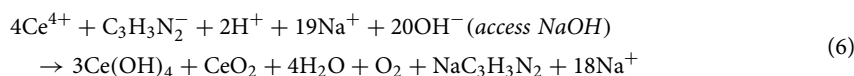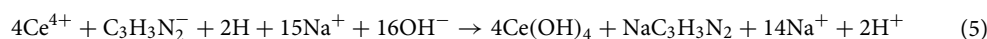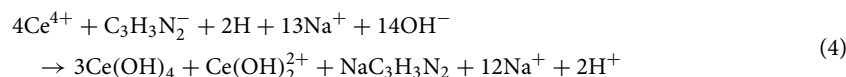
Figure 3. High-resolution TEM images of super-fine wet ceria abrasives with synthesis termination pH values of (**a**) 4.0, (**b**) 4.5, (**c**) 5.0, (**d**) 5.5, (**e**) 6.0, and (**f**) 6.5. The background TEM images were obtained at a 50-nm scale (lower left), whereas the TEM images in the insets of the figures (upper right) were observed at a 2-nm scale. In addition, a μ-crystalline diffraction pattern of super-fine wet ceria abrasives were presented in the inset of the figures (upper left), shown in Fig. S6.

associated with the dependencies of the chemical composition of the synthesized abrasives and the secondary abrasive size on the synthesis termination pH.

The morphology of the $Ce(OH)_4$ or CeO_2 abrasives dependent on the synthesis termination pH was observed using high-resolution(HR) transmission electron microscopy (TEM). At a pH of 4.0, the $Ce(OH)_4$ abrasives were well crystallized, and the average and standard deviation of their size were 2.06 and 0.15 nm, respectively; these are referred to as super-fine wet ceria abrasives, as shown in the HR-TEM image in Fig. 3a. In addition, their u-diffraction pattern exhibited a typical polycrystalline diffraction pattern with a higher intensity sequence of (111), (220), (311), (200), (400), (331), and (420), as shown in the u-diffraction pattern of Fig. 3a. This diffraction pattern was consistent with the crystalline planes and higher intensity sequence of crystalline wet ceria abrasives produced by a typical wet precipitation method at 60–80 °C, as shown in Fig. S2. Up to a pH of 5.0, the size and crystalline planes of the $Ce(OH)_4$ abrasives appeared constant, as shown in Figs. 3a–c and S6a–c. The size of the mixture of the $Ce(OH)_4$ and CeO_2 abrasives increased very slightly with the synthesis termination pH; however, their polycrystalline planes were similar to that of the $Ce(OH)_4$ abrasives, as shown in Figs. 3d–f and S6d–f. Therefore, super-fine wet ceria abrasives ~ 2 nm in size were synthesized at temperature of 25 °C using only a Ce^{4+} precursor.

To understand whether $Ce(OH)_4$ or CeO_2 abrasives were synthesized, the chemical reaction equations of super-fine wet ceria abrasives are reviewed in detail as follows:

$$4(NH_4)_2Ce(NO_3)_6 + H_2O \rightarrow 4[Ce(NO_3)_6]^{2-} + 8NH^{4+} + OH^- + H^+ \tag{1}$$

$$\begin{aligned} 4[Ce(NO_3)_6]^{2-} &+ 8NH^{4+} + OH^- + H^+ + C_3H_4N_2 \\ &\rightarrow 4Ce^{4+} + 24NO^{3-} + 8NH^{4+} + OH^- + C_3H_3N_2^- + 2H^+ \end{aligned} \tag{2}$$

$$\begin{aligned} 4Ce^{4+} &+ C_3H_3N_2^- + 2H^+ + 11Na^+ + 12OH^- \\ &\rightarrow 3Ce(OH)_4 + Ce^{4+} + NaC_3H_3N_2 + 10Na^+ + 2H^+ \end{aligned} \tag{3}$$

4

$$4Ce^{4+} + C_3H_3N_2^- + 2H + 13Na^+ + 14OH^-$$
$$\rightarrow 3Ce(OH)_4 + Ce(OH)_2^{2+} + NaC_3H_3N_2 + 12Na^+ + 2H^+ \tag{4}$$

$$4Ce^{4+} + C_3H_3N_2^- + 2H + 15Na^+ + 16OH^- \rightarrow 4Ce(OH)_4 + NaC_3H_3N_2 + 14Na^+ + 2H^+ \tag{5}$$

$$4Ce^{4+} + C_3H_3N_2^- + 2H^+ + 19Na^+ + 20OH^- \, (access\ NaOH)$$
$$\rightarrow 3Ce(OH)_4 + CeO_2 + 4H_2O + O_2 + NaC_3H_3N_2 + 18Na^+ \tag{6}$$

$$4Ce^{4+} + C_3H_3N_2^- + 2H^+ + 27Na^+ + 28OH^- \, (access\ NaOH)$$
$$\rightarrow Ce(OH)_4 + 3CeO_2 + 14H_2O + 6O_2 + NaC_3H_3N_2 + 26Na^+ \tag{7}$$

$$4Ce^{4+} + C_3H_3N_2^- + 2H^+ + 31Na^+ + 32OH^- \, (access\ NaOH)$$
$$\rightarrow 4CeO_2 + 16H_2O + 4O_2 + NaC_3H_3N_2 + 30Na^+. \tag{8}$$

The dissolution of ammonium cerium nitrate (i.e., $(NH_4)_2Ce(NO_3)_6$) as a precursor to DI water produces $[Ce_9NO_3)_6]^{2-}$, NH^{4+}, OH^-, and H^+, which exhibits a transparent orange color, as shown in Eq. (1) and (i) in Fig. 2a. The addition of imidazole ($C_3H_4N_2$) into the solution in Eq. (1) as a catalyst enhances the solubility of Ce^{4+}, and the solution then exhibits a transparent and bright yellow color, as shown in Eq. (2) and beaker (iii) of Fig. 2a. Between pH values of 4.0 and 5.0 (region I), the addition of NaOH as a synthesis termination titrant produces the $Ce(OH)_4$ abrasives, and a higher synthesis termination pH (i.e., NaOH titrant amount) leads to a higher solid loading weight of the $Ce(OH)_4$ abrasives. Additionally, the synthesized abrasives exhibited a bright yellow color, as shown in Eq. (3)–(5), beakers (i) and (iii) of Figs. 2b, and S3a–c. However, between the pH values of 5.5 and 6.0, further addition of the NaOH titrant generates a mixture of $Ce(OH)_4$ and CeO_2 abrasives; thus, a larger amount of NaOH titrant results in more CeO_2 abrasives than $Ce(OH)_4$ abrasives, as shown in Eq. (6) and (7), beakers (iv) and (v) of Figs. 2b, and S3d–e. Moreover, at a pH of 6.5, further addition of the NaOH titrant primarily generates the CeO_2 abrasives, which are completely sediment after adding the NaOH titrant to the synthesized solution, as shown in Eq. (8), beaker (vi) of Figs. 2b and S3f. Thus, between the pH values of 5.5 and 6.5 (region II), the abrasive solid loading concentration significantly decreased with increasing synthesis termination pH, and the abrasive color changed from dark yellow to pale yellow and dark pale yellow, as shown in Figs. 2c, S3d–f. The chemical reaction equations of the super-fine wet ceria abrasive synthesis dependent on the synthesized pH clearly explain the synthesis mechanism of super-fine (~2 nm in size) wet ceria abrasives, and the precise chemical composition of super-fine wet ceria abrasives are extremely sensitive to the synthesis termination pH.

Dependency of SiO_2-film polishing rate on synthesis termination pH of super-fine wet ceria abrasives.

The synthesized wet ceria abrasives (i.e., facet-surface CeO_2 abrasives) produced by a conventional wet precipitation method at 60–80 °C generally encounters an extreme limitation regarding the trade-off between the SiO_2-film polishing rate and the remaining scratches after CMP, which is dependent on the wet ceria abrasive size; that is, a smaller wet ceria abrasive size leads to a lower SiO_2-film polishing rate and fewer remaining scratches after CMP, as shown in Fig. 1. To achieve minimal stick-and-slip type scratches induced by a SiO_2-film CMP using conventional facet-surface wet ceria-abrasives, the wet abrasive size must be less than 3 nm. However, its SiO_2-film polishing rate performed less than 10 nm/min for a 300-mm-diameter SiO_2-film CMP, which cannot be applied for the CMP process for nanoscale semiconductor devices. Thus, whether or not the super-fine (~2 nm in size) wet ceria abrasive ($Ce(OH)_4$, mixture of CeO_2 and $Ce(OH)_4$, or CeO_2 abrasives) CMP slurries can overcome the trade-off hurdle of a conventional facet-surface wet ceria abrasive (i.e., CeO_2 abrasives) is an essential factor in determining the possibility of applying them for the CMP process of nanoscale semiconductor devices.

First, to investigate the dependency of the SiO_2-film polishing rate on the synthesis termination pH of super-fine wet ceria abrasives, the SiO_2-film CMP slurries were fabricated using 0.3 wt% super-fine wet ceria abrasives, a dispersant (0.3 wt% polyvinyl alcohol (PVA)), and DI water, a titrant (NaOH) adjusted at a pH of 6.0 of the CMP slurries, as a function of the synthesis termination pH. It was previously mentioned that super-fine wet ceria abrasives were centrifuged three times after synthesis at different termination pH values. Then, all abrasives were again dispersed with PVA and titrated at a pH of 6.0 using NaOH and DI water. The CMP slurry color varied from transparent yellow to opaque yellow when the synthesis termination pH increased from 4.0 to 6.5, as shown in the beakers in Fig. 4a. From a pH of 4.0 to 4.5 (region I), the peak absorbance wavelength of all CMP slurries was ~293 nm. However, from a pH of 5.0 to 6.5 (region II), this value increased from 299 to 300 and 302 nm when the synthesis termination pH increased from 5.0 to 5.5 and 6.5, as shown in the inset of Fig. 4a. Additionally, the peak absorbance decreased from 1.397 to 1.099 a.u. when the synthesis termination pH increased from 4.0 to 6.0, and it then abruptly increased to 1.303 at a pH of 6.5. This behavior is similar to the dependency of the peak absorbance of super-fine wet ceria abrasives on the synthesis termination pH in Fig. 2b. In region I, the zeta potential of the super-fine wet ceria abrasive-based CMP slurries rapidly decreased from +18.1 to +11.40 mV when the synthesis termination pH increased from 4.0 to 5.0. In region II, it reached ~+11.0 mV as the pH increased further, as shown in Fig. 4b. Thus, the abrasive zeta potential exhibited two different regions of dependence on the synthesis termination pH: region I (i.e., zeta potential decrease) and region II (i.e., saturated zeta
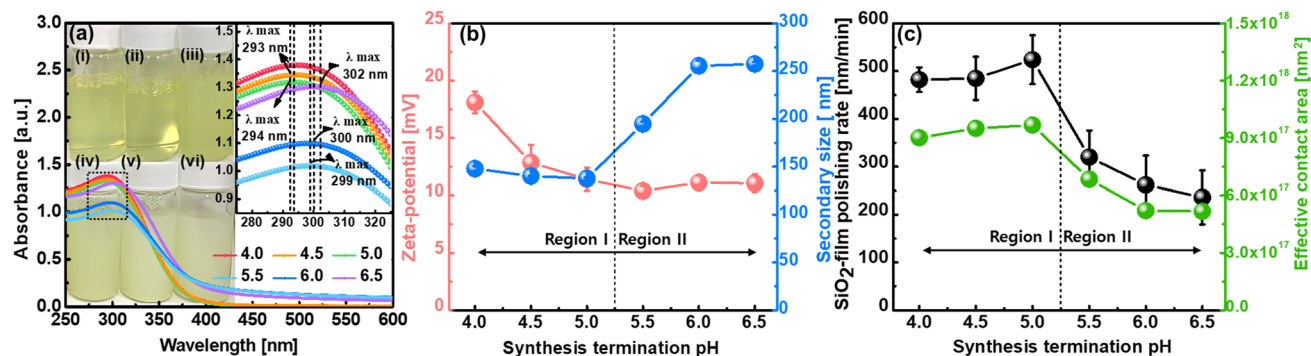
Figure 4. CMP slurry characteristics and CMP performance dependent on synthesis termination pH. (**a**) Peak absorption wavelength and absorbance, (**b**) abrasive zeta potential and secondary abrasives size, and (**c**) SiO_2-film polishing rate and effective contact area between abrasives and SiO_2-film surface. In (**a**), the CMP slurries in beakers (i), (ii), (iii), (iv), (v), and (vi) were terminated at pH values of 4.0, 4.5, 5.0, 5.5, 6.0, and 6.5, respectively, following a synthesis.

potential). Moreover, in region I, the secondary abrasive size of the CMP slurries decreased very slightly from 147 to 137 nm when the synthesis termination pH increased from 4.0 to 5.0; however, in region II, it rapidly increased from 195 to 258 nm when the synthesis termination pH increased from 5.5 to 6.5. Hence, the secondary abrasive size also exhibited two different regions of dependence on the synthesis termination pH: region I (i.e., almost constant secondary abrasive size) and region II (i.e., rapid increase in secondary abrasive size). Note that the secondary abrasive size in a CMP slurry responds to the dispersant degree of the primary abrasives (i.e., super-fine wet ceria abrasives), which directly affects the film polishing rate. A larger secondary abrasive in a CMP slurry generally leads to a lower SiO_2-film polishing rate[35–40]. Furthermore, in region I, the 12-inch-wafer SiO_2-film polishing rate slightly increased from 482 to 524 nm/min when the synthesis termination pH increased from 4.0 to 5.0. In region II, it rapidly decreased from 524 to 236 nm/min for a further increase in the synthesis termination pH, as shown in Fig. 4c. This result indicates that there were also two different regions of dependence in the 12-inch-wafer SiO_2-film polishing rate on the synthesis termination pH: region I (i.e., slight SiO_2-film polishing rate increase) and region II (i.e., rapid SiO_2-film polishing rate decrease). The region where two regions coincided can be understood by considering three points of view (i.e., abrasive zeta potential, secondary-abrasive size, and effective contact area between abrasives and the SiO_2-film surface). In region I, the SiO_2-film polishing rate slightly increased with decreasing abrasive zeta potential and the secondary abrasive size of the CMP slurries because a high attractive static force between the $Ce(OH)_4$ abrasives and the SiO_2-film surface led to a lower SiO_2-film polishing rate and a larger secondary abrasive size in the CMP slurry, which resulted in a lower SiO_2-film polishing rate[35–40]. Note that the zeta potentials of the SiO_2-film surface and $Ce(OH)_4$ abrasives are highly negatively charged (~ -28.8 mV) and positively charged ($+11.4$ to $+18.1$ mV), respectively; thus, the static force between the abrasives and the SiO_2-film surface is a strong attractive force. In region II, the SiO_2-film polishing rate abruptly decreased above a pH of 5.0 because the secondary abrasive composition transferred from $Ce(OH)_4$ at a pH of 5.0 to the mixture of $Ce(OH)_4$ at a pH of 5.5; therefore, the secondary abrasive size significantly increased from 137 to 195 nm. Additionally, when the synthesis termination pH increased from 5.5 to 6.5, the SiO_2-film polishing rate decreased considerably with the synthesis termination pH because the secondary abrasive size in the CMP slurries increased significantly with the termination pH. Furthermore, the dependence of the SiO_2-film polishing rate on the synthesis termination pH was in good agreement with that of the effective contact area between the abrasives and the SiO_2-film surface on the synthesis termination pH, as shown in Fig. 4c. Note that the effective contact area between the abrasives and the SiO_2-film surface was calculated with the assumption that the morphology of super-fine wet ceria secondary abrasives is spherical, and the abrasives are at the fixed abrasive solid loading (0.3 wt%) as a function of the synthesis termination pH. In a SiO_2-film CMP process, for planarization of the SiO_2-film surface topography, the secondary-abrasives in a CMP slurry touch and rub the $Si(OH)_x$ layer produced by hydrolysis reaction. Hence, the contact area of the secondary-abrasives determines the SiO_2-film polishing-rate; i.e., a larger total contact-area leads to a higher SiO_2-film polishing-rate, called contact-area based on CMP mechanism, as shown in Fig. S7. If the solid loading of the abrasives in a SiO_2-film CMP slurry is fixed with 0.3 wt%, a larger secondary-abrasive size in the CMP slurry would lead to a smaller number of secondary-abrasives in the slurry, indicating that the total contact-area of the CMP slurry having a small secondary-abrasive size would be larger than that having a large secondary-abrasive size. As a result, the SiO_2-film polishing-rate using the slurry with a small secondary-abrasive size would be higher than that using the slurry with a large secondary-abrasive size. These results prove that the dependence of the SiO_2-film polishing rate on the synthesis termination pH are related to the abrasive zeta potential, secondary abrasive size, and total abrasive SiO_2-film-surface contact area. Interestingly, the super-fine (~ 2 nm in size) wet ceria abrasive ($Ce(OH)_4$ abrasive)-based CMP slurry achieved minimal stick-and-slip type scratches after the 12-inch-wafer SiO_2-film CMP, as shown in Fig. S1c. Additionally, the SiO_2-film polishing rate (~ 524 nm/min) of super-fine (~ 2 nm in size) wet ceria abrasive ($Ce(OH)_4$ abrasive)-based CMP slurry was ~ 50 times higher than that (~ 10 nm/min) of the facet surface (~ 3 nm in size) wet ceria abrasive (CeO_2 abrasive)-based CMP slurry.
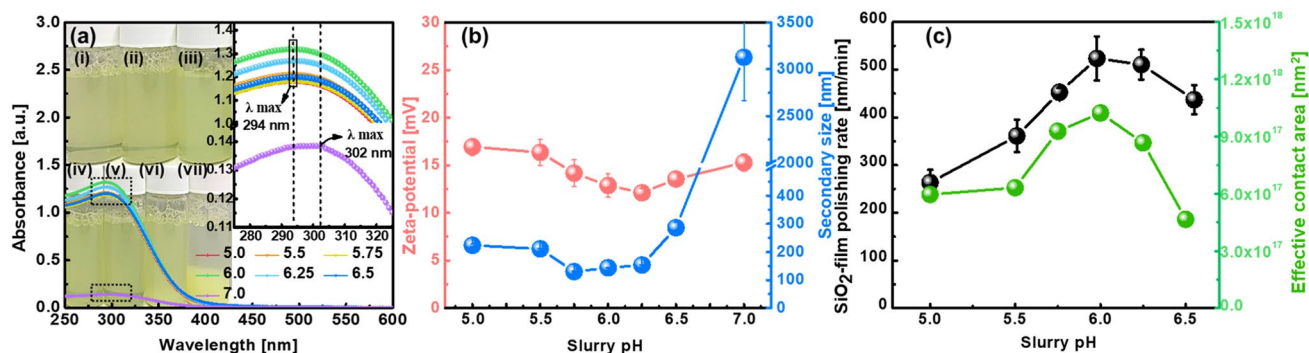
Figure 5. CMP slurry characteristics and CMP performance dependent on pH values of slurries, including super-fine (~2 nm in size) $Ce(OH)_4$ wet ceria abrasives. (**a**) Peak absorption wavelength and absorbance, (**b**) abrasive zeta potential and secondary abrasives size, and (**c**) SiO_2-film polishing rate and effective contact area between abrasives and SiO_2-film surface. In (**a**), the CMP slurries in beakers (i), (ii), (iii), (iv), (v), and (vi) were produced at pH values of 5.0, 5.25, 5.5, 5.75, 6.0, 6.5, and 7.0, respectively, following a synthesis. As previously mentioned, super-fine wet ceria abrasives for all CMP slurries were synthesized at a termination pH of 5.0.

Dependency of SiO_2-film polishing rate on pH of super-fine wet ceria abrasives-based CMP slurry.

Because the SiO_2-film CMP slurries that include super-fine wet ceria abrasives (~2 nm $Ce(OH)_4$ abrasives) exhibited a maximum SiO_2-film polishing rate at the synthesis termination pH of 5.0, the dependency of the SiO_2-film polishing rate on the CMP slurry pH was investigated at a solid loading of 0.3 wt% and a dispersant (PVA) concentration of 0.25 wt%. Excluding the CMP slurry with a pH of 7.0, those with pH values between 5.0 and 6.5 exhibited a transparent yellow color, and their abrasives were well dispersed in the slurry, as shown in beakers (i)–(vi) of Fig. 5a. However, the abrasives in the CMP slurry with a pH of 7.0 were completely sediment. Moreover, excluding the CMP slurry with a pH of 7.0, the absorbance of the CMP slurry with pH values between 5.0 and 6.5 peaked at a wavelength of 294 nm. However, the peak absorbance of the CMP slurry at a pH of 7.0 was identified at a wavelength of 302 nm, owing to the sedimentation of abrasives in the CMP slurry. The peak absorbance of the CMP slurries slightly increased with the CMP slurry pH at 5.0–6.0; however, it considerably decreased with increasing CMP slurry pH at 6.25–7.0, as shown in the inset of Fig. 5a. This is similar to the dependence of the peak absorbance on the synthesis termination pH in the inset of Fig. 4a. The abrasive zeta potential of the CMP slurry decreased slightly from +16.9 to +12.1 mV when the CMP slurry pH increased from 5.0 to 6.25, and it increased weakly from +12.1 to +15.3 mV for further CMP slurry pH increase, as shown Fig. 5b. This result implies that the lowest abrasive zeta potential (+12.11 mV) was observed at a specific pH (6.25). Additionally, the secondary abrasive size decreased considerably from 223 to 130 nm when the CMP slurry pH increased from 5.0 and 6.0, and it increased significantly from 153 to 3126 nm when the pH increased from 6.25 to 7.0. This result indicates that the minimum secondary abrasive size (130 nm), which has an excellent dispersant degree, was identified at a specific pH (6.0). As a result of the dependencies of the abrasive zeta potential and secondary abrasive size on the CMP slurry pH, the SiO_2-film polishing rate significantly increased from 263 to 524 nm/min when the CMP slurry pH increased from 5.0 to 6.0, and then decreased considerably from 524 to 437 nm as the CMP slurry pH increased further, as shown in Fig. 5c. Additionally, the dependency of the SiO_2-film polishing rate on the CMP slurry pH was well correlated with that of the abrasive effective contact area on the SiO_2-film surface, that is, a higher effective contact area led to a higher SiO_2-film polishing rate. Thus, the super-fine $Ce(OH)_4$ abrasive-based CMP slurry demonstrated an excellent abrasive dispersant characteristic and a superior SiO_2-film CMP performance (i.e., stick-and-slip type, scratch-free, and SiO_2-film polishing rate > ~500 nm/min) at a CMP slurry pH of 5.0–6.0. However, its SiO_2-film polishing rate was sensitive to the CMP slurry pH, The SiO_2-film polishing rate rapidly increased with the CMP slurry pH; the ratio of the SiO_2-film polishing rate to the slurry pH was 84 nm/min per pH). In addition, the surface roughness of the SiO_2-film surface before and after CMP were estimated by AFM, as shown in Fig. S8. The scanning area of AFM was 5 μm × 5 μm and the surface roughness was calculated by using root-mean-square (Rq). The surface roughness of the SiO_2-film surface before CMP was 0.394-nm, while those after CMP at pH 5.00, 5.50, 5.75, 6.00, 6.25 and 6.50 were 0.360, 0.376, 0.342, 0.359, 0.366 and 0.316-nm, respectively. These result indicate that there was no degradation of the SiO_2-film surface roughness by CMP.

Discussion

To achieve minimal stick-and-slip type scratches and a high polishing rate with a SiO_2-film CMP in nanoscale semiconductor devices, super-fine wet ceria abrasives were synthesized via a novel wet precipitation process using Ce^{4+} and a catalyst enhancing Ce^{4+} soluble at temperature of 25 °C. This is in contrast to the conventional wet precipitation that uses a mixture of Ce^{4+} with Ce^{3+} and an amine-based synthesized catalyst at 60–80 °C. The chemical composition of super-fine wet ceria abrasives strongly depended on the synthesis termination pH: $Ce(OH)_4$ abrasives at a pH of 4.0–5.0 and a mixture of $Ce(OH)_4$ with CeO_2 at a pH of 5.5–6.5. The $Ce(OH)_4$ abrasives were well dispersed in a SiO_2-film CMP solution, and exhibited a transparent yellow color; however, the CeO_2 abrasives, which exhibit an opaque yellow color, were significantly agglomerated in the CMP solution. As a result, $Ce(OH)_4$ abrasives with excellent dispersant ability were identified at a specific synthesis termination

pH (5.0), which presented the minimum positively charged abrasive zeta potential (~ 12 mV) and the minimum secondary abrasive size (~ 130 nm). Additionally, super-fine Ce(OH)$_4$ wet ceria abrasives crystallized well with an f.c.c crystalline structure and an average size of ~ 2 nm. Although the abrasive size is only several nanometers, the super-fine abrasive-based SiO$_2$-film CMP slurry exhibited a high SiO$_2$-film polishing rate (> 500 nm/min), owing to the extremely high population of super-fine abrasives and excellent dispersion ability. Additionally, it could achieve a surface free of stick-and-slip type scratches after a SiO$_2$-film CMP. It should be noted that a conventional CeO$_2$ dry or wet ceria abrasive is not free of CMP-induced scratches. Furthermore, the abrasive zeta potential and secondary abrasive size in the CMP slurries, including super-fine wet ceria abrasives, were very sensitive to the CMP slurry pH, and principally determined the CMP performance, such as the SiO$_2$-film polishing rate and CMP induced scratches. The best CMP performance with a minimum abrasive zeta potential (~ 13 mV) and abrasive secondary size (~ 130-nm in size) could be achieved at a specific CMP slurry pH (6.0), which was different from the synthesis termination pH (5.0). The sensitive pH characteristic of the super-fine abrasive-based SiO$_2$-film CMP slurry enabled the study of the stability of the CMP slurry. Additionally, further chemical design studies to achieve a low cost (i.e., dependency of solid loading on CMP performance) and self-stop CMP function (i.e., polishing rate selectivity between SiO$_2$-, Si$_3$N$_4$-, and poly-Si-films) are essential for various CMP applications in nanoscale semiconductor devices.

Methods

Ce(OH)$_4$ abrasive synthesis.

For super-fine wet ceria synthesis, 0.052 mol of (NH$_4$)$_2$Ce(NO$_3$)$_6$ was dissolved in DI water. The initial pH of the (NH$_4$)$_2$Ce(NO$_3$)$_3$ solution was 1.30, and the solution was dark orange in color. This indicates that (NH$_4$)$_2$Ce(NO$_3$)$_6$ is dissociated in DI water and exists as [Ce(NO$_3$)$_6$]$^{2-}$ and NH^{4+}. Additionally, 0.170 mol of C$_3$H$_4$N$_2$ was dissolved in DI water to enhance Ce^{4+} solubility. The pH of the C$_3$H$_4$N$_2$ solution was 11.4, and the solution was colorless. Then, the C$_3$H$_4$N$_2$ solution was added to the (NH$_4$)$_2$Ce(NO$_3$)$_6$ solution at a rate of 10 ml/min for 15 min. All these synthesis processes were conducted at temperature of 25 °C and maintained at a constant stirring rate. After the C$_3$H$_4$N$_2$ and (NH$_4$)$_2$Ce(NO$_3$)$_6$ solutions were mixed, the final pH and color of the solution were 3.01 and transparent bright yellow, respectively. Through this color change, it could be inferred that the (NH$_4$)$_2$Ce(NO$_3$)$_6$ solution is completely ionized to Ce^{4+} by comparison with the color when the C$_3$H$_4$N$_2$ solution was not added. After synthesis, the mixture of the (NH$_4$)$_2$Ce(NO$_3$)$_6$ and C$_3$H$_4$N$_2$ solutions was titrated to a specific pH (4.0–6.5) using NaOH as the titrant. The solution was then centrifuged three cycles at 8000 rpm.

Materials.

The CMP slurries used in this study were composed of 0.3 wt% super-fine wet ceria abrasives, a pH titrant (NaOH), a dispersant (PVA), and DI water. F.c.c. crystalline Ce(OH)$_4$ was synthesized as an abrasive particle with a primary particle diameter of ~ 2 nm. Ammonium cerium (IV) nitrate ((NH$_4$)$_2$Ce(NO$_3$)$_3$, Junsei Chemical, Tokyo, Japan) was used as the precursor material for the synthesis of Ce(OH)$_4$ abrasive particles. Additionally, imidazole (C$_3$H$_4$N$_2$, Sigma Aldrich, St. Louis, Missouri, USA) was used as a catalyst to improve the solubility of (NH$_4$)$_2$Ce(NO$_3$)$_3$. Sodium hydroxide (NaOH, Junsei Chemical, Tokyo, Japan) was used to adjust the pH. PVA (Polysciences, Warrington, US) was used as a dispersant. The slurry was prepared with the following concentration: 0.3 wt% nano-scale Ce(OH)$_4$ abrasives and 0.3 wt% PVA dispersant. The pH of the slurry was titrated at 6.0 using NaOH.

CMP conditions.

The 450-nm SiO$_2$-film were prepared on a 12-inch-diameter Si wafer with CVD. The sample was polished using a polisher (POLI-762, G&P Tech. Inc., Republic of Korea) with an industry standard CMP pad of polyurethane-like (IC1000/Suba IV, Rohm & Haas Electronic Materials, USA). Before polishing, the polishing pad was conditioned with a diamond disk and DIW for 30 min, and then polished 3 dummy SiO$_2$-film wafers. When evaluating slurries of different conditions, pad conditioning was performed for 15 min, and 3 dummy SiO$_2$-film wafers were polished using DIW to remove the previous slurry from the pad. The applied polishing pressure was 3 PSI and the rotation speed of the wafer carrier and the table were set to 93 and 87 rpm/ min, respectively. The flow rate of the slurry was kept at 200 mL/min, and the polishing time was set at 60 s.

Characterization.

The morphology of the abrasive particles was observed using HR-TEM (JEM-2010, JEOL, Tokyo, Japan) with an accelerating voltage of 200 kV. To investigate the dispersant degree of the SiO$_2$-film CMP slurry, the absorbance of the abrasives at 292–302 nm was measured using ultraviolet-visual spectroscopy (Cary 5000, VARIAN, Palo, Alto, CA, USA). Additionally, the zeta potential and diameter of the secondary particles were analyzed using a particle analyzer (ELSZ2+, Otsuka Electronics, Osaka, Japan) with electrophoresis techniques and dynamic light scattering. For measuring the secondary abrasive diameter of a CMP slurry, the slurry was diluted until the solid loading of CMP slurry was 0.3 wt% and then the 1 ml of the diluted CMP slurry was loaded at a particles counter (ELS-Z). The thickness of the SiO$_2$-film was measured using ellipsometry (V-VASE, J.A. Woollam Co., Inc., Lincoln, NE, USA). The polishing rate of the SiO$_2$-film was calculated by subtracting the SiO$_2$-film thickness after CMP from that before CMP. At all CMP slurries in our experimental, 3 times CMP were conducted with three 300-mm-diameter SiO$_2$-film wafers and 149 points with 6.1-mm interval and 1-mm exclusion from wafer edge were measured for each of wafers. In our experiment, there were no other factors impacting the CMP SiO$_2$-film polishing-rate.

Data availability

The datasets generated during and/or analyzed during the current study are available from the corresponding author on reasonable request.

References

1. Li, Y. 3D NAND memory and its application in solid-state drives: Architecture, reliability, flash management techniques, and current trends. *IEEE Solid-State Circuits Mag.* **12**(4), 56–65. https://doi.org/10.1109/MSSC.2020.3021841 (2020).
2. Maejima, H. *et al.* A 512Gb 3b/Cell 3D flash memory on a 96-word-line-layer technology. In *IEEE International Solid State Circuits Conference—(ISSCC)* 336–338, https://doi.org/10.1109/ISSCC.2018.8310321 (2018).
3. Micheloni, R., Aritome, S. & Crippa, L. Array architectures for 3-D NAND flash memories. *IEEE* **105**, 1634–1649. https://doi.org/10.1109/JPROC.2017.2697000 (2017).
4. Goda, A. 3-D NAND technology achievements and future scaling perspectives. *IEEE Trans. Electron Devices* **67**, 1373–1381. https://doi.org/10.1109/TED.2020.2968079 (2020).
5. Kim, S. K. & Popovici, M. Future of dynamic random-access memory as main memory. *Mater. Adv. Semicond. Mem.* **43**(5), 334–339. https://doi.org/10.1557/mrs.2018.95 (2018).
6. Parat, K. & Dennison, C. A floating gate based 3D NAND technology with CMOS under array. In *IEEE International Electron Devices Meeting (IEDM)* 3.3.1–3.3.4, https://doi.org/10.1109/IEDM.2015.7409618 (2015).
7. James, D. & Choe, J. *TechInsights Memory Technology Update from IEDM18*, https://www.techinsights.com/blog/techinsights-memory-technology-update-iedm18, Posted: April 11 (2019).
8. Chandrasekaran, N., Ramaswamy, N. & Mouli, C. Memory technology: Innovations needed for continued technology scaling and enabling advanced computing systems. In *IEEE International Electron Devices Meeting (IEDM)* 10.1.1–10.1.8, https://doi.org/10.1109/IEDM13553.2020.9372125 (2020).
9. den Brink, M. V. Continued scaling in semiconductor manufacturing enabled by advances in lithography. In *IEEE International Electron Devices Meeting (IEDM)* 1.2.1–1.2.5. https://doi.org/10.1109/IEDM19573.2019.8993590 (2019).
10. Courtland, R. Moore's law's next step: 10 nanometers. *IEEE Spectr.* **54**(1), 52–53. https://doi.org/10.1109/MSPEC.2017.7802750 (2017).
11. Moore, S. K. Another step toward the end of Moore's law: Samsung and TSMC move to 5-nanometer manufacturing. *IEEE Spectr.* **56**(6), 9–10. https://doi.org/10.1109/MSPEC.2019.8727133 (2019).
12. Liu, C. & Chang, Y. Simultaneous EUV flare- and CMP-aware placement. In *IEEE 32nd International Conference on Computer Design (ICCD)* 249–255, https://doi.org/10.1109/ICCD.2014.6974689 (2014).
13. Hasan, R. M. M. & Luo, X. Promising lithography techniques for next-generation logic devices. *Nanomanuf. Metrol.* **1**, 67–81. https://doi.org/10.1007/s41871-018-0016-9 (2018).
14. Chiang, H. K., Liu, C., Jiang, J. R. & Chang, Y. Simultaneous EUV flare variation minimization and CMP control by coupling-aware dummification. *IEEE Trans. Comput. Aided Des. Integr. Circuits Syst.* **35**(4), 598–610. https://doi.org/10.1109/TCAD.2015.2488492 (2016).
15. Okazaki, S. High resolution optical lithography or high throughput electron beam lithography: The technical struggle from the micro to the nano-fabrication evolution *Microelectron. Eng.* **133**, 23–35, ISSN 0167-9317, https://doi.org/10.1016/j.mee.2014.11.015 (2015).
16. Kato, H. *et al.* Sub-30nm via interconnects fabricated using directed self-assembly, *Microelectron. Eng.* **110**, 152–155, ISSN 0167-9317, https://doi.org/10.1016/j.mee.2013.03.025 (2013).
17. Takeno, Y. & Okamoto, K. New market trend in CMP equipment/material for the "More than Moore" era. In *International Conference on Electronics Packaging and iMAPS All Asia Conference (ICEP-IAAC)* 423–425, https://doi.org/10.23919/ICEP.2018.8374338 (2018).
18. Tsai, S. *et al.* CMP: Consideration of stop-on selectivity in advanced node semiconductor manufacturing technology. *ECS Trans.* https://doi.org/10.1149/07704.0169ecst (2017).
19. Zhang, K. Effect of chelating agent and ammonium dodecyl sulfate on the interfacial behavior of copper CMP for GLSI. *ECS J. Solid State Sci. Technol.* **7**, P509. https://doi.org/10.1149/2.0231809jss (2018).
20. Ghulghazaryan, R. G., Piliposyan, D. G., Shoyan, M. T. & Nersisyan, H. V. Application of machine learning-based electrochemical deposition models to CMP modeling. *Math. Probl. Comput. Sci.* **53**, 39–48. https://doi.org/10.51408/1963-0051 (2020).
21. Khanna, A. J. *et al.* Impact of pad material properties on CMP performance for sub-10nm technologies. *ECS J. Solid State Sci. Technol.* https://doi.org/10.1149/2.0121905jss (2019).
22. Li, T. C. *et al.* CMP solutions for 3D-NAND staircase CMP. In *International Conference on Planarization/CMP Technology (ICPT)* 1–3 (2015).
23. Huang, H. *et al.* New CMP processes development and challenges for 7nm and beyond. In *China Semiconductor Technology International Conference (CSTIC)* (2018).
24. Meng, Y. *et al.* Impact of bevel condition on STI CMP scratch. In *China Semiconductor Technology International Conference (CSTIC)* 1–2 (2020).
25. Wortman-Otto, K. M. *et al.* Role of molecular structure on modulating the interfacial dynamics for shallow trench isolation (STI) chemical mechanical planarization (CMP). *ECS J. Solid State Sci. Technol.* **10**, 024009. https://doi.org/10.1149/2162-8777/abe7aa (2021).
26. Bai, F., Zhang, Z., Wang, J. & Wang, H. Impact of wafer transfer process on STI CMP scratches. In *China Semiconductor Technology International Conference (CSTIC)* 1–4 (2017).
27. Yang, J. C., Penigalapati, D., Chao, T.F., Lu, W.Y. & Koli, D. Challenges in chemical mechanical planarization defects of 7nm device and its improvement opportunities. In *China Semiconductor Technology International Conference (CSTIC)* 1–3 (2017).
28. Wang, C. *et al.* Role of slurry chemistry for defects reduction during barrier CMP. In *China Semiconductor Technology International Conference (CSTIC)* 1–3 (2020).
29. Mukherjee, S. & Aggarwal, G. Metal CMP process optimization for low abrasive slurry. In *Annual SEMI Advanced Semiconductor Manufacturing Conference (ASMC)* 226–230 (2018).
30. Chen, K. -W. *et al.* STI scratch defects reduction by using solid pad in 1X technology node. In *China Semiconductor Technology International Conference (CSTIC)* 1–3 (2018).
31. Oh, D., Kim, H., Han, M., Hwang, H. & Kim, T. The experimental study on relationship between shape of diamond and micro scratches. In *Proceedings of International Conference on Planarization/CMP Technology* 158–161 (2014).
32. Pettinger, N. W., Williams, R. E. A., Chen, J. & Kohler, B. Crystallization kinetics of cerium oxide nanoparticles formed by spontaneous, room-temperature hydrolysis of cerium(IV) ammonium nitrate in light and heavy water. *Phys. Chem. Chem. Phys.* **19**, 3523–3531. https://doi.org/10.1039/c6cp08227k (2017).
33. Veranitisagul, C. *et al.* Novel recovery of nano-structured ceria (CeO_2) from Ce(III)-benzoxazine dimer complexes via thermal decomposition. *Int. J. Mol. Sci.* **12**, 4365–4377. https://doi.org/10.3390/ijms12074365 (2011).
34. Nurhasanah, I., Safitri, W., Arifin, Z., Subagio, A. & Windarti, T. Antioxidant activity and dose enhancement factor of CeO_2 nanoparticles synthesized by precipitation method. *Mater. Sci. Eng.* **432**, 012031. https://doi.org/10.1088/1757-899X/432/1/012031 (2018).

35. Wang, Y., Zhao, Y., An, W., Ni, Z. & Wang, J. Modeling effects of abrasive particle size and concentration on material removal at molecular scale in chemical mechanical polishing. *Appl. Surf. Sci.* **257**, 249–253, ISSN 0169-4332, https://doi.org/10.1016/j.apsusc.2010.06.077 (2010).
36. Zeng, T. & Sun, T. Size effect of nanoparticles in chemical mechanical polishing—A transient model. *IEEE Trans. Semicond. Manuf.* **18**(4), 655–663 (2005).
37. Werrell, J. M. *et al.* Effect of slurry composition on the chemical mechanical polishing of thin diamond films. *Sci. Technol. Adv. Mater.* https://doi.org/10.1080/14686996.2017.1366815 (2017).
38. Seo, E.-B. *et al.* Influence of scavenger on abrasive stability enhancement and chemical and mechanical properties for tungsten-film chemical-mechanical-planarization. *ECS J. Solid State Sci. Technol.* **9**, 065001. https://doi.org/10.1149/2162-8777/ab9fe5 (2020).
39. Seo, E.-B. *et al.* Interfacial chemical and mechanical reactions between tungsten-film and nano-scale colloidal zirconia abrasives for chemical-mechanical-planarization. *ECS J. Solid State Sci. Technol.* **9**, 054001. https://doi.org/10.1149/2162-8777/ab915c (2020).
40. Yun, S.-S. *et al.* Dishing-free chemical mechanical planarization for copper films. *Colloids Surf. A* **616**, 126143. https://doi.org/10.1016/j.colsurfa.2021.126143 (2021).

Acknowledgements

Author contributions

Y.H.S. and J.G.P. conceived and designed the study. Y.H.S. synthesis all abrasives and carried out experiments, with the help of J.G.P. Data measurements and organization were contributed by Y.H.S., G.P.J., P.S.K., M.H.H. and S.W.H. J.Y.B., S.I.K. and J.H.P. participated fundamental data search and analysis. All authors contributed to discussions regarding the research. Y.H.S. and J.G.P. analyzed the all data and wrote the manuscript.

Competing interests

The authors declare no competing interests.

Additional information

Supplementary Information The online version contains supplementary material available at https://doi.org/10.1038/s41598-021-97122-9.

Correspondence and requests for materials should be addressed to J.-G.P.

Reprints and permissions information is available at www.nature.com/reprints.

Publisher's note Springer Nature remains neutral with regard to jurisdictional claims in published maps and institutional affiliations.